Diffusive spreading and mixing of fluid monolayers

2005 J. Phys.: Condens. Matter 17 S4189

(http://iopscience.iop.org/0953-8984/17/49/013)

INSTITUTE OF PHYSICS PUBLISHING JOURNAL OF PHYSICS: CONDENSED MATTER

J. Phys.: Condens. Matter **17** (2005) S4189–S4198 doi:10.1088/0953-8984/17/49/013

Diffusive spreading and mixing of fluid monolayers

M N Popescu[1,2,4], **S Dietrich**[1,2] **and G Oshanin**[1,2,3]

[1] Max-Planck-Institut für Metallforschung, Heisenbergstraße 3, 70569 Stuttgart, Germany
[2] Institut für Theoretische und Angewandte Physik, Universität Stuttgart, Pfaffenwaldring 57, 70569 Stuttgart, Germany
[3] Laboratoire de Physique Théorique des Liquides, Université Paris 6, 4 Place Jussieu, 75252 Paris, France

E-mail: popescu@mf.mpg.de, dietrich@mf.mpg.de and oshanin@lptl.jussieu.fr

Received 30 June 2005
Published 25 November 2005
Online at stacks.iop.org/JPhysCM/17/S4189

Abstract

The use of ultra-thin, i.e. monolayer, films plays an important role in the emerging field of nano-fluidics. Since the dynamics of such films is governed by the interplay between substrate–fluid and fluid–fluid interactions, the transport of matter in nanoscale devices may eventually be efficiently controlled by substrate engineering. For such films, the dynamics is expected to be captured by two-dimensional lattice-gas models with interacting particles. Using a lattice-gas model and the non-linear diffusion equation derived from the microscopic dynamics in the continuum limit, we study two problems of relevance in the context of nano-fluidics. The first one is the case in which along the spreading direction of a monolayer a mesoscopic-sized obstacle is present, with a particular focus on the relaxation of the fluid density profile upon encountering and passing the obstacle. The second one is the mixing of two monolayers of different particle species which spread side by side following the merger of two chemical lanes, here defined as domains of high affinity for fluid adsorption surrounded by domains of low affinity for fluid adsorption.

1. Introduction

There are substantial efforts to miniaturize chemical processes by using microfluidic systems. The 'lab on a chip concept' integrates a great variety of chemical and physical processes into a single device in a similar way as an integrated circuit incorporates many electronic devices into a single chip [1]. These microfluidic devices not only allow for cheap mass production but they can operate with much smaller quantities of reactants and reaction products than standard laboratory equipment. This is particularly important for solutions containing rare and expensive substances, such as certain biological materials, and for toxic or explosive components [2].

[4] Author to whom any correspondence should be addressed.

Even though most microfluidic devices available today have micron sized channels, further miniaturization is leading towards the nanoscale [2, 3]. Besides meeting technical challenges, new theoretical concepts are needed to understand the basic physical processes underlying this new technology [4–6]. Whereas the ultimate limits for miniaturization of electronic devices are set by quantum fluctuations, in a chemical chip these limits are determined by thermal fluctuations and can be explored by methods of classical statistical mechanics.

At the sub-micron thickness scale, recent experiments of liquid spreading on atomically smooth surfaces [7–9], performed with volumes of the order of nanolitres, have clearly shown by means of dynamic ellipsometry or x-ray reflectivity measurements that precursor films with *molecular thickness* and *macroscopic extent* advance in front of the macroscopic liquid wedge of the spreading drop. (Thin, i.e., of the order of 100 nm, precursor films spreading ahead of the macroscopic droplet have also been observed experimentally [10].) The occurrence of molecularly thin precursor films with a similar spreading dynamics has also been evidenced very recently for immiscible metal systems in three regimes: solid drops with a solid film, solid drops with a liquid film, and liquid drops with a liquid film [11, 12]. Theoretical work (see [13–16] and references therein) combined with an impressive number of molecular dynamics (MD) and Monte Carlo (MC) simulations (see [17] and references therein) addressed the mechanisms behind the extraction and the experimentally observed $t^{1/2}$ asymptotic time dependence of the linear extent of the precursor films on chemically homogeneous substrates [7, 13, 15, 18]. This led to a good understanding of the spreading dynamics and of the intrinsic morphology of the films. Based on these results, more complicated issues can be addressed such as, e.g., the spreading behaviour of monolayers exposed to chemically patterned substrates [19, 20], or the question of mixing of different fluids at the nano-scale that we shall present below.

The organization of the paper is as follows. In section 2 we briefly present the lattice gas model of interacting particles and discuss the rules defining the microscopic dynamics and the nonlinear diffusion equation derived from it in the continuum limit. Section 3 is devoted to a qualitative discussion of the results obtained for the case of monolayer spreading in the presence of mesoscopic obstacles, with a particular focus on the relaxation of the density profile upon encountering and passing the obstacle. In section 4 we discuss the mixing of two species during spreading of monolayers following the merger of two chemical lanes, and we conclude with a brief summary of the results in section 5.

2. Fluid monolayers on homogeneous substrates

Recently, we have studied the structure of a monolayer which is extracted from a reservoir [18] and spreads on a flat, chemically homogeneous substrate, by using a lattice gas model of interacting particles as proposed in [14, 15]. Since we shall use this model as a starting point for our present study, for clarity and further reference we briefly describe the defining rules of the model and the non-linear diffusion equation obtained from the microscopic dynamics within the continuum limit. A thorough analysis of this model is presented in [18].

(a) We choose a homogeneous substrate such that the spreading occurs in the x–y plane. The half-plane $x < 0$ is occupied by a reservoir of particles at fixed chemical potential which maintains at its contact line with the substrate—positioned at the line $x = 0$—an *average* density C_0 (defined as the number of particles per unit length in the transversal y direction). At time $t = 0$, the half-plane $x > 0$ is empty. There is no imposed flow of particles from the reservoir pushing the extracting film.

(b) The substrate–fluid interaction is modelled as a periodic potential forming a lattice of potential wells with coordination number z ($z = 4$ for a square lattice) and lattice

constant a. The particle motion proceeds via activated jumps between nearest-neighbour wells; evaporation from the substrate is not allowed. The activation barrier U_A determines the jumping rate $\Omega = \nu_0 \exp[-U_A/k_B T]$, where ν_0 is an attempt frequency defining the time unit, k_B is the Boltzmann constant, and T is the temperature.

(c) The pair interaction between fluid particles at distance r is taken to be hard-core repulsive at short range, preventing double occupancy of the wells, and attractive at long range, $-U_0/r^6$ for $r \geqslant 1$, resembling a Lennard-Jones type interaction potential. Here and in the following all distances are measured in units of the lattice constant a and therefore are dimensionless. The selection of the nearest-neighbour well into which a particle attempts to jump, i.e., the probability $p(\boldsymbol{r} \to \boldsymbol{r}'; t)$ that a jump from location $\boldsymbol{r}$ will be directed toward the location $\boldsymbol{r}'$, is biased by the fluid–fluid energy landscape and is given by

$$p(\boldsymbol{r} \to \boldsymbol{r}'; t) = \frac{\exp\left\{\frac{\beta}{2}[\tilde{U}(\boldsymbol{r}; t) - \tilde{U}(\boldsymbol{r}'; t)]\right\}}{Z(\boldsymbol{r}; t)}, \tag{1}$$

where $Z(\boldsymbol{r}; t) = \sum_{\boldsymbol{r}', |\boldsymbol{r}'-\boldsymbol{r}|=1} \exp\{\frac{\beta}{2}[\tilde{U}(\boldsymbol{r}; t) - \tilde{U}(\boldsymbol{r}'; t)]\}$ is the normalization constant and $1/\beta = k_B T$,

$$\tilde{U}(\boldsymbol{r}; t) = -U_0 \sum_{\boldsymbol{r}', 0<|\boldsymbol{r}'-\boldsymbol{r}|\leqslant 3} \frac{\eta(\boldsymbol{r}'; t)}{|\boldsymbol{r} - \boldsymbol{r}'|^6}, \tag{2}$$

and $\eta(\boldsymbol{r}'; t) \in \{0, 1\}$ is the occupation number of the well at $\boldsymbol{r}'$ at the time t. The summation in equation (2) has been restricted to three lattice units for computational convenience. This corresponds to the cut-off generally used in molecular dynamics simulations for algebraically decaying Lennard-Jones pair potentials. The rates

$$\omega_{\boldsymbol{r}\to\boldsymbol{r}';t} = \Omega p(\boldsymbol{r} \to \boldsymbol{r}'; t) \tag{3}$$

for the transitions from $\boldsymbol{r}$ to neighbouring sites $\boldsymbol{r}'$ satisfy

$$\sum_{\boldsymbol{r}', |\boldsymbol{r}'-\boldsymbol{r}|=1} \omega_{\boldsymbol{r}\to\boldsymbol{r}';t} \equiv \Omega. \tag{4}$$

Thus for any given particle at any location the total rate of leaving a potential well is determined only by the fluid–solid interaction characterized by U_A, is time independent, and equals Ω.

Neglecting all spatial and temporal correlations, i.e., assuming that averages of products of occupation numbers $\eta(\boldsymbol{r}; t)$ are equal to the corresponding products of averaged occupation numbers $\rho(\boldsymbol{r}; t) = \langle \eta(\boldsymbol{r}; t) \rangle$, where $\langle \cdots \rangle$ denotes the average with respect to the corresponding probability distribution $\mathcal{P}(\{\eta(\boldsymbol{r}; t)\})$ of a configuration $\{\eta(\boldsymbol{r}; t)\}$, one can formulate a mean-field master equation for the local occupational probability, i.e., the number density $\rho(\boldsymbol{r}; t)$ [18]. In the continuum limit of space and time ($\Delta t \to 0$, $a \to 0$, $\Omega^{-1} \to 0$, $D_0 = \Omega a^2/4$ finite) for the master equation, by taking Taylor expansions for $p(\boldsymbol{r} \to \boldsymbol{r}')$ and $\rho(\boldsymbol{r}'; t)$ around $\boldsymbol{r}$ and keeping terms up to second-order spatial derivatives of the density $\rho(\boldsymbol{r}; t)$ [18, 21], one obtains the following nonlinear and *nonlocal* equation for $\rho(\boldsymbol{r}; t)$ [22, 23]:

$$\partial_t \rho = D_0 \nabla [\nabla \rho + \beta \rho (1 - \rho) \nabla U] + \mathcal{O}(a^2) \tag{5}$$

where

$$U(\boldsymbol{r}; t) \equiv \langle \tilde{U}(\boldsymbol{r}; t) \rangle = -U_0 \sum_{\boldsymbol{r}'', 0<|\boldsymbol{r}''-\boldsymbol{r}|\leqslant 3} \frac{\rho(\boldsymbol{r}''; t)}{|\boldsymbol{r}'' - \boldsymbol{r}|^6} \tag{6}$$

is replacing $\tilde{U}(\boldsymbol{r}; t)$ in the definition (1) for $p(\boldsymbol{r} \to \boldsymbol{r}')$.

Being nonlinear and, due to the term involving the interaction potential $U(\boldsymbol{r}; t)$, nonlocal, equation (5) cannot be solved analytically and in most of the cases even the computation of a

numerical solution is a difficult task. However, assuming that the density $\rho(\boldsymbol{r};t)$ is a slowly varying function of the spatial coordinates the potential $U(\boldsymbol{r};t)$ may be expanded as

$$U(\boldsymbol{r};t) = -U_0 \sum_{\boldsymbol{r}',0<|\boldsymbol{r}'-\boldsymbol{r}|\leqslant 3} \frac{\rho(\boldsymbol{r}';t)}{|\boldsymbol{r}'-\boldsymbol{r}|^6}$$
$$\simeq -U_0\rho(\boldsymbol{r};t) \sum_{\boldsymbol{r}',0<|\boldsymbol{r}'-\boldsymbol{r}|\leqslant 3} \frac{1}{|\boldsymbol{r}'-\boldsymbol{r}|^6} + \mathcal{O}(a^2), \tag{7}$$

which leads to the *local* equation

$$\partial_t\rho = D_0\nabla\{[1 - gW_0\rho(1-\rho)]\,\nabla\rho\} + \mathcal{O}(a^2), \tag{8}$$

where $W_0 = \beta U_0$, and $g = \sum_{1\leqslant|\boldsymbol{r}|\leqslant r_c} |\boldsymbol{r}|^{-6}$ is a geometrical factor depending on the lattice type (e.g., square, triangular, etc) and on the cut-off range of the potential. For the present case of a square lattice and a cut-off at $r_c = 3$ one has $g \simeq 4.64$.

Rescaling time as $t \to \tau = D_0 t$ and defining an effective diffusion coefficient,

$$D_e(\rho) = 1 - gW_0\rho(1-\rho), \tag{9}$$

equation (8) may be written in the usual form of a diffusion equation:

$$\partial_\tau\rho = \nabla\,[D_e(\rho)\nabla\rho] + \mathcal{O}(a^2). \tag{10}$$

The functional form of $D_e(\rho)$ (equation (9)) implies that for $W_0 > 4/g$ there will be values ρ_i of the density for which $D_e(\rho_i) < 0$. For parameters such that $W_0 < 4/g$, equation (10) is a proper diffusion equation (though non-linear), while for $W_0 > 4/g$ instabilities are expected in the range of densities for which $D_e(\rho_i) < 0$, i.e., for $\rho_i \in (\rho_\alpha^-, \rho_\alpha^+)$ where

$$\rho_\alpha^\pm = \frac{1}{2}\left(1 \pm \sqrt{1 - \frac{4}{gW_0}}\right). \tag{11}$$

It is known [22, 24–26] that these instabilities lead to discontinuities in the density profile ('shocks'), i.e., they correspond to the formation of sharp interfaces. For the model defined by rules (a)–(d), the value for the threshold interaction strength for which such interfaces emerge is predicted by the continuum theory as $W_0^{(t)} = 4/g \simeq 0.86$, which is significantly smaller than the lower bound estimate $W_0^{(t)} > 1$ from KMC simulations. We attribute this to the mean-field character of the derivation of the continuum equation. Therefore it is necessary to include particle–particle correlations in the mean-field description. Since the dynamics is possible only by jumps into empty sites, one can argue that for $z = 4$ the summation in g should include at most three contributions from nearest neighbour sites. This leads to $g \simeq 3.64$ and an estimate for the threshold interaction $W_0^{(t)} \simeq 1.1$, in good agreement with the KMC results. For the rest of the analysis we shall use this corrected value of g. Additional support for this corrected value is provided by the analysis of the density profiles [18].

The constraint, that the reservoir keeps the mean density at $x = 0$ at a fixed value C_0, implies the boundary condition

$$\rho(x = 0, y; t) = C_0. \tag{12}$$

Depending on the particular system under study, additional boundary conditions may have to be satisfied. For example, for the case studied in [18], in the absence of formation of interfaces, i.e., for interactions $W_0 < W_0^{(t)}$ and for large times, the density on the advancing edge $X(t)$ could be considered as fixed and equal to C_1,

$$\rho(x = X(t), y; t) = C_1, \tag{13}$$

where $C_1 = 0.11$ as inferred from the kinetic Monte Carlo (KMC) simulations. (This boundary condition (equation (13)) naturally occurred also in the theory of Burlatsky *et al* [15].) For

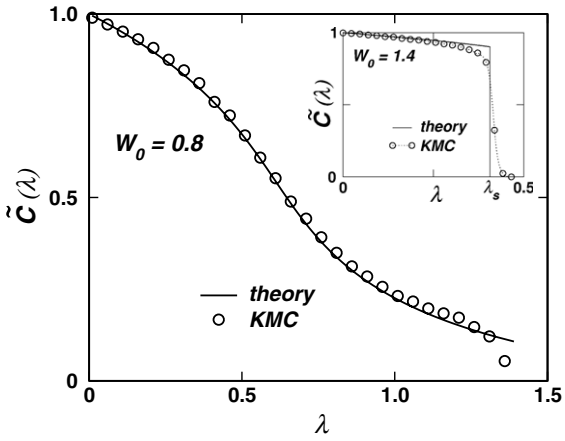

Figure 1. Asymptotic scaling solution $\rho(x,t) = \tilde{C}(\lambda)$ for $W_0 = 1.0$ (regular solution) and (see the inset) $W_0 = 1.4$ (shock solution) with $\lambda = x/\sqrt{D_0 t}$. The theoretical results are obtained from equation (10) (solid lines). The KMC results (open circles) correspond to the time $t = 2 \times 10^6$ (in units of ν_0^{-1}) which is close to the asymptotic limit (see [18]). λ_s denotes the position of the discontinuity as obtained by analytical theory [18].

that system, the absence of boundaries along the y-direction and the y-independence of the boundary conditions at $x = 0$ and $x = X(t)$ leads to an effectively one-dimensional problem and to a scaling solution $\rho(x,t) = \tilde{C}(\lambda = x/\sqrt{t})$. The analysis of equation (10) depends on whether $W_0 < W_0^{(t)}$ or $W_0 > W_0^{(t)}$. As shown in [18], in both cases the solutions are in excellent agreement with those obtained from KMC simulations; typical results are shown in figure 1. While for the liquid-on-solid systems mentioned in the introduction these intrinsic density profiles have not been measured yet, data of such density profiles are available for the immiscible metal systems studied in [11, 12] and they are at least in good qualitative agreement with the theoretical ones. Since the present model appears to provide a simple but realistic description of a fluid monolayer spreading on a homogeneous substrate, it is natural to use it as a starting point to address more complex problems, such as the spreading of monolayers on *designed* chemically heterogeneous substrates, or the mixing of monolayers.

3. Diffusive spreading around mesoscopic obstacles

In order to apply the model described in section 2 to study the spreading of a monolayer around a mesoscopic-size obstacle, we add to rules (a)–(d) in section 2 the following ones.

(e) The obstacle is taken to be a square-shaped domain $\mathcal{D}$ of side length h centred at $(x = d \geqslant h/2, y = 0)$ (see also figure 2(a)). This domain is composed of sites with very low affinity for the fluid particles. The activation barrier $U_{\mathcal{D}}$ for jumps from sites outside $\mathcal{D}$ to those inside $\mathcal{D}$ is taken to be much larger than U_{A}, such that the boundary $\partial\mathcal{D}$ of $\mathcal{D}$ acts effectively as a hard wall.

(f) A sink reservoir occupies the region $x \geqslant L$, where $L \gg 1$ and $L \gg d + h$, and maintains at its contact line with the substrate, positioned at the line $x = L$, an *average* density (number of particles per unit length in the transversal y direction) $C_1 = 0$.

Under these assumptions, the density profile $\rho(x, y, t)$ as the solution of equation (10) fulfils the initial condition

$$\rho(x, y, 0) = C_0 \Theta(-x), \tag{14}$$

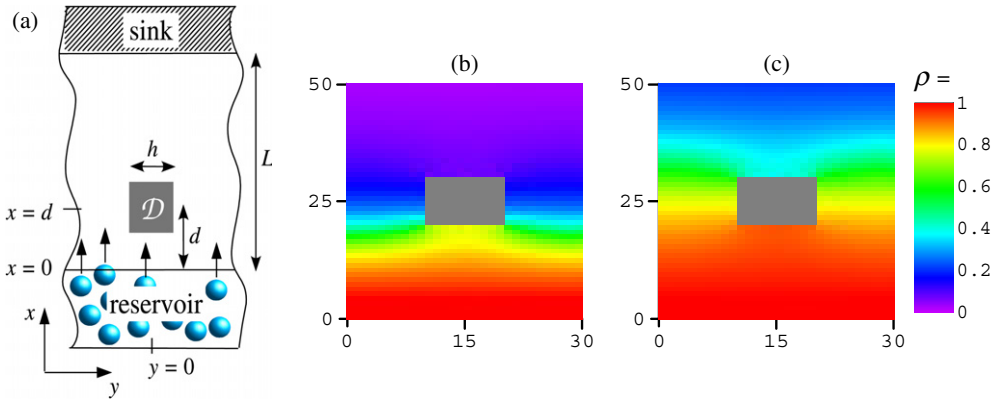

Figure 2. (a) Schematic drawing of a substrate with high affinity for fluid adsorption patterned with a square domain $\mathcal{D}$ (length h, centred at $(x = d \geqslant h/2, y = 0)$) of very low affinity for fluid adsorption obstructing the spreading. The substrate is in contact with a reservoir of particles located at $x \leqslant 0$ from which a monolayer is extracted and spreads along the x direction. A sink of particles is located at $x = L$. There are periodic boundary conditions in the y-direction. (b), (c) Density profiles in the vicinity of the obstacle from numerical integration of equation (10) with initial and boundary conditions given by equations (14)–(16), respectively, for a spreading monolayer whose edge just encounters an obstacle ($\tau = 200$) (b) and has just passed the obstacle ($\tau = 2000$) (c). The parameters used in the simulations are $C_0 = 1.0$, $W_0 = 0.9$, $d = 20$, $h = 10$, $L_x = 200$, $L_y = 30$. The right box shows the colour coding for the density.

where $\Theta(x)$ denotes the Heaviside step function, and the boundary conditions

$$\begin{aligned} &\rho(0, y, t) = C_0, \\ &\rho(L, y, t) = 0, \\ &\boldsymbol{j}_n|_{\partial\mathcal{D}} = 0. \end{aligned} \tag{15}$$

The current $\boldsymbol{j}$ is given by (see equation (10))

$$\boldsymbol{j} = -D_{\mathrm{e}}(\rho)\nabla\rho. \tag{16}$$

Note that in a numerical study the system necessarily has a finite size L_y along the y direction. We will use periodic boundary conditions and sizes $L_y \gg 1$ such that $h/L_y < 1$ but not negligible (mesoscopic-size obstacle) and $L_y - h \gg r_{\mathrm{c}}$, such that the boundary $\partial\mathcal{D}$ of the obstacle is sufficiently far away from the edge of the simulation box to avoid finite-size effects.

In figures 2(b) and (c) we present typical results for the density profiles in the vicinity of the obstacle obtained from the numerical integration of equation (10) with initial and boundary conditions given by equations (14)–(16), respectively, for a spreading monolayer whose edge just encounters an obstacle ($\tau = 200$) (b) and has just passed the obstacle ($\tau = 2000$) (c). Several conclusions can be drawn from visually inspecting figures 2(b) and (c). Upon approaching the obstacle, the boundary condition of zero normal current at the boundary of the obstacle (reflecting wall) leads to an increase in the density in a region at the front of the spreading monolayer, as shown by the forward bending of the iso-density lines (see, e.g., the yellow band in figure 2(b)). Upon passing the front edge of the obstacle, the iso-density lines become straight, and once they reach the end of the obstructed region they bend again, this time backwards. This indicates that upon passing the obstacle the spreading tends to proceed faster in the regions far from the obstacle, while at the obstacle the iso-density lines are pinned until they cover the whole edge on the back of the obstacle (see, e.g., the light blue

band neighbouring the green region in figure 2(c)). Once this is realized, the iso-density line detaches from the back edge of the obstacle, and the bending slowly relaxes (see, e.g., the boundary between the light and dark blue regions in the top region of figure 2(c)), while the spreading continues; far away from the obstacle, the iso-density lines become again straight.

We end this section by noting that the maximum linear extent of the region where the iso-density lines are deformed, as well as the survival time of these deformations, can be used as quantitative measures to describe the relaxation of the density perturbations induced by the obstacle as a function of the inter-particle attractive interactions, as well as of the scaled size h/L_y of the mesoscopic obstacle (assuming that this is the most relevant geometrical parameter). The results of this analysis will be the subject of a forthcoming paper.

4. Diffusive mixing of two fluid monolayers composed of different species

The model described in section 2 can be used to study the mixing of two spreading fluid monolayers composed of different species A and B, if one assumes that the two species interact with the substrate in such a way that the same lattice structure of potential wells, eventually with different depths (i.e., different escape rates Ω_i), can accommodate both types of species. Assuming a square lattice of lattice constant a and assuming the on-site hard core repulsion between any two particles such that double occupancy remains forbidden, the equations satisfied by the densities $\rho_j(x,t)$, where $j \in \{\mathrm{A},\mathrm{B}\}$, are obtained from equation (5) by replacing U with $U_{ii}+U_{ij}$, where U_{ii} is the potential due to same-species interactions while U_{ij}, $j \neq i$, is the potential due to interactions between different species, D_0 with $D_i = \Omega_i a^2/4$, and changing the single-occupancy term from $1-\rho(\boldsymbol{r},t)$ to $1-\rho_{\mathrm{A}}(\boldsymbol{r},t)-\rho_{\mathrm{B}}(\boldsymbol{r},t)$:

$$\partial_t \rho_i = D_i \nabla \left[\nabla \rho_i + \beta \rho_i (1-\rho_i-\rho_j) \nabla (U_{ii}+U_{ij}) \right], \qquad i,j \in \{\mathrm{A},\mathrm{B}\}, \quad j \neq i. \tag{17}$$

We note here that there is no summation over the same indices, and we also note that in the case of identical species, i.e., $D_{\mathrm{A}} = D_{\mathrm{B}}$ and $U_{\mathrm{AA}} = U_{\mathrm{BB}} = U_{\mathrm{AB}}$, by adding equation (17) for $i = A$ and the corresponding one for $i = B$ one finds that as expected the density $\rho = \rho_{\mathrm{A}} + \rho_{\mathrm{B}}$ satisfies equation (5). Assuming that the long-ranged parts of the pair interactions A–A, B–B, and A–B are of the same Lennard-Jones form (see section 2) only with different strengths $U_0^{(ij)}$, $i, j \in \{\mathrm{A},\mathrm{B}\}$, one can repeat the same argument as that following equation (5) to reduce equation (17) to a *local* one,

$$\partial_t \rho_i = D_i \nabla \left[\nabla \rho_i - g \rho_i (1-\rho_i-\rho_j)(W_{ii} \nabla \rho_i + W_{ij} \nabla \rho_j) \right], \qquad i,j \in \{\mathrm{A},\mathrm{B}\}, \quad j \neq i, \tag{18}$$

where the notation $W_{ij} = \beta U_0^{(ij)}$ has been introduced.

We consider a T-junction patterned onto a planar, rectangular substrate of size $L_x \times 2L_y$ as described below (see also figure 3(a)). The spreading monolayers are extracted from reservoirs of particles A and B, respectively, which maintain constant line densities $C_0^{\mathrm{A,B}}$ at the lines $\mathcal{C}_1 = (y = -L_y, 0 \leqslant x \leqslant d)$ and $\mathcal{C}_2 = (y = L_y, 0 \leqslant x \leqslant d)$, respectively. The domains $\mathcal{D}_1 = \{(x,y) | y < -h/2 \wedge x > d\}$ and $\mathcal{D}_2 = \{(x,y) | y > h/2 \wedge x > d\}$ represent sites with very low affinity for the fluid particles of either type, such that similarly to the situation in section 3 the boundaries of these domains effectively act as hard walls, confining the spreading onto the two lanes forming the inverted T-junction. Finally, we assume that at the foot $x = L_x$, $|y| \leqslant h/2$ of the T-junction there is a sink for particles of both species. Under these assumptions, the functions $\rho_{\mathrm{A,B}}(x,y,t)$ as solutions of equation (18) fulfil the initial

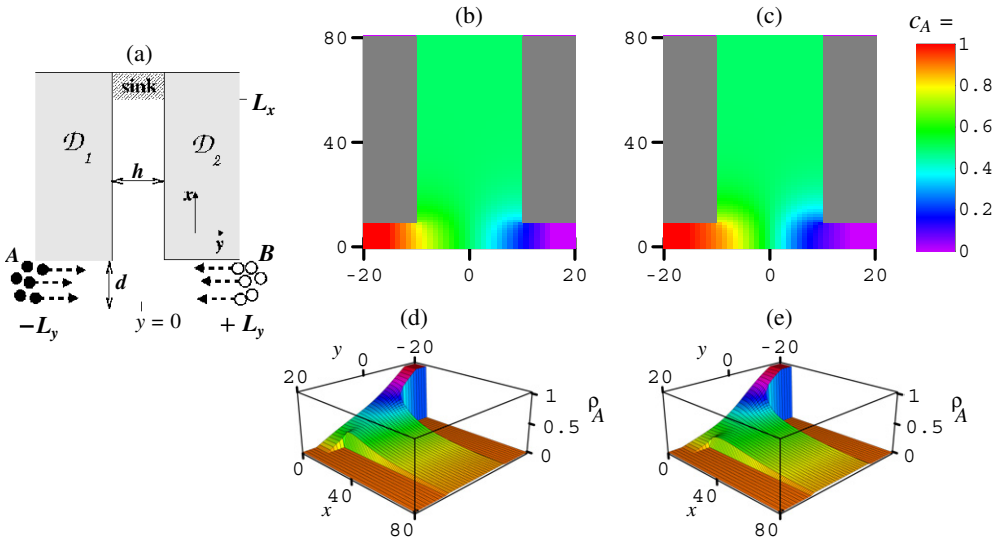

Figure 3. (a) Schematic drawing of a T-shaped pattern with high affinity for a fluid in contact with two reservoirs for particles of species A and B, located at $y = -L_y$ and $y = L_y$, respectively. The two monolayers spread initially in opposite directions along the y axis, and upon meeting they start to mix and to invade the empty stripe of width h located at $x > d, |y| \leqslant h/2$. The rectangular domains $\mathcal{D}_1$ and $\mathcal{D}_2$ consist of sites with very low affinity for fluid adsorption. A sink of particles is located at $x = L_x$. (b), (c) Results for the mixing parameter $c_A(\boldsymbol{r}, \tau)$ near the T-junction from numerical integration of equation (18) with initial and boundary conditions given by equations (20) and (21) for the cases of attractive inter-species interaction $W_{AB} = 0.6$ (b) and repulsive inter-species interaction $W_{AB} = -0.6$ (c), respectively, at $\tau = 10^3$, for $W_{AA} = W_{BB} = 0.7$, and $C_0^A = C_0^B = 1.0$. (d), (e) Results for the density $\rho_A(\boldsymbol{r}, \tau)$ of A particles for attractive inter-species interaction $W_{AB} = 0.6$ (d) and repulsive inter-species interaction $W_{AB} = -0.6$ (e). The other parameters are the same as in (b) and (c). Note that there is no colour-coding for $\rho_A(\boldsymbol{r}, \tau)$.

condition

$$\begin{aligned} &\rho_A(x, y, 0) = C_0^A, && (x, y) \in \mathcal{C}_1, \\ &\rho_B(x, y, 0) = C_0^B, && (x, y) \in \mathcal{C}_2, \\ &\rho_{A,B}(x, y, 0) = 0, && \text{otherwise}, \end{aligned} \tag{19}$$

and the boundary conditions

$$\begin{aligned} &\rho_A(x, y, t)|_{\mathcal{C}_1} = C_0^A, \\ &\rho_B(x, y, t)|_{\mathcal{C}_2} = C_0^B, \\ &\rho_A(L_x, y, t) = \rho_B(L_x, y, t) = 0, \\ &j_n^{A,B}|_{\partial\mathcal{D}_{1,2}} = 0, \end{aligned} \tag{20}$$

where the current $\boldsymbol{j}^A$ ($\boldsymbol{j}^B$ is obtained by exchanging the labels A $\leftrightarrow$ B) is now given by (see equation (18))

$$\boldsymbol{j}^A = \nabla\rho_A - g\rho_A(1 - \rho_A - \rho_B)(W_{AA}\nabla\rho_A + W_{AB}\nabla\rho_B). \tag{21}$$

In the following we focus on the effect of the A–B interaction on the dynamics of mixing of otherwise identical monolayers, i.e., we choose $W_{AA} = W_{BB}$, $D_A = D_B$, and $C_0^A = C_0^B$; the results discussed in the following correspond to the particular choice $C_0^A = C_0^B = 1$, while the parameter D_A is absorbed into the variable $\tau = D_A t$. The geometrical parameters are fixed to

$L_x = 500$, $L_y = 20$, and $d = h = 20$. The mixing will be characterized by the ratio

$$c_A(\boldsymbol{r}, \tau) = \frac{\rho_A(\boldsymbol{r}, \tau)}{\rho_A(\boldsymbol{r}, \tau) + \rho_B(\boldsymbol{r}, \tau)} \tag{22}$$

(with the convention $c_A = 0$ if $\rho_A + \rho_B = 0$), which is close to unity in A-rich regions, close to zero in B-rich regions, and close to one-half in regions where mixing is accomplished (i.e., $\rho_A \simeq \rho_B \neq 0$).

In figures 3(b) and (c) we present typical results for $c_A(\boldsymbol{r}, \tau)$ from numerical integration of the coupled set of equations given by equation (18) with the initial and boundary conditions equations (20) and (21) for the case of attractive interactions $W_{AA} = W_{BB} = 0.7$ and attractive inter-species interaction $W_{AB} = 0.6$ (b), respectively repulsive inter-species interaction $W_{AB} = -0.6$ (c). From these figures it is clear that within the stripe forming the leg of the T-junction there is almost perfect mixing.

Surprisingly, at first glance the result seems to be almost independent of the sign of the A–B interaction, and there is only a weak dependence on the strength W_{AB} of this interaction, except for the extension of the A-rich and B-rich regions near the corners of the T-junction. However, this behaviour can be easily rationalized in view of the fact that, as shown in [18], the structure and dynamics of the spreading of a one-component monolayer of particles with inter-particle attraction $W_{AA} = 0.7$ is also well described by the 'effective boundary force' theory of Burlatsky *et al* [15], which disregards interactions within the bulk of the monolayer. The reason for this is that the density in the spreading monolayer is relatively low, except for the region near the reservoir, and thus the system is too dilute to be influenced by the inter-particle attraction. Therefore, in the initial stages of spreading and mixing, the stripe is invaded by low density phases of A and B which mix independently of their mutual interaction. This scenario is well supported by the comparative analysis of the corresponding density profiles $\rho_A(\boldsymbol{r}, \tau)$ in the cases $W_{AB} = 0.6$ and $W_{AB} = -0.6$, respectively, shown in figures 3(d) and (e): almost everywhere in the stripe the density of A particles is low, in the range of 0–0.25, and thus the mixture behaves as a dilute, non-interacting two-dimensional gas. Finally, we note a weak dependence of the extension of the A-rich and B-rich regions near the corners of the T-junction on the sign of the W_{AB} interaction (compare figures 3(b) and (c), respectively (d) and (e)).

The above scenario holds for all values $W_{AA} = W_{BB} \leqslant 0.9$ and $|W_{AB}| \leqslant W_{AA}$ that we have tested, and thus the (tentative) conclusion is that the symmetric T-geometry would ensure practically perfect mixing (but without any possibility of controlling the spatial extent or the spatial distribution of mixing) for two-component monolayers with a similarity of the interactions between like species. However, further calculations should be carried out before definite conclusions can be drawn concerning this issue. For example, for the case $W_{AA}, W_{BB} > 1.1$ we expect sharp interfaces to emerge in each of the two spreading monolayers, which might eliminate the 'mixing through the low density front' mechanism discussed above. Simulations for these ranges of values for the inter-particle interactions turned out to be extremely time consuming, and work is still in progress to elucidate this point.

5. Summary

A lattice gas model of interacting particles and the corresponding nonlinear diffusion equation derived from its microscopic dynamics in the continuum limit provide a simple but realistic description of fluid monolayer spreading on a homogeneous substrate. Based on previous results for spreading on a homogeneous substrate, here we have extended this model to address two more complex problems: the spreading of monolayers around obstacles (section 3) and the mixing of monolayers (section 4). These are simple examples of spreading on chemically *designed* substrates.

For the case of monolayer spreading in the presence of a mesoscopic obstacle, the results obtained from the numerical integration of the nonlinear diffusion equation (equation (10)) with initial and boundary conditions given by equations (14)–(16) show that the iso-density lines are bent and pinned by the obstacle during the spreading of the monolayer around it. For a fixed geometry, a fixed density of the reservoir, and fixed substrate–fluid and inter-particle interactions the spatial and temporal extent of this bending in front of and behind the obstacle can be used as measures for the relaxation of the density profile upon passing around the obstacle.

As an example for the mixing of two species in the course of spreading of two monolayers at the merger of two chemical lanes, we have discussed the case of a T-junction geometry. We have focused on the effect of the A–B inter-species interaction on the dynamics of mixing of otherwise identical monolayers. Surprisingly, so far our results lead to the conclusion that the symmetric T-geometry together with the similarity of the same-species interaction ensures practically perfect mixing (but without any possibility of controlling the spatial extent or the spatial distribution of mixing) for two monolayers of different species, independently of the sign or the strength of the A–B interaction. Only the extension of the A-rich and B-rich regions near the corners of the T-junction exhibits differences. This behaviour reflects the fact that in the initial stages of spreading and mixing the stripe is invaded by low density phases of A and B, which mix independently of the inter-species interaction; the resulting mixture is a dilute, quasi-non-interacting two-dimensional gas. Because this complete mixing has occurred at early stages, when repulsion does not play a role, and since the continuum equation does not contain any noise terms, demixing or segregation is not observed in the present calculations, although it is expected to occur for strongly repulsive A–B interactions.

References

[1] Giordano N and Cheng J-T 2001 *J. Phys.: Condens. Matter* **13** R271
[2] Mitchell P 2001 *Nat. Biotechnol.* **19** 717
[3] Stone H A and Kim S 2001 *AIChE J.* **47** 1250
[4] Dietrich S 1998 *J. Phys.: Condens. Matter* **10** 11469
[5] Zhao B, Moore J S and Beebe D J 2002 *Anal. Chem.* **74** 4259
[6] Dietrich S, Popescu M N and Rauscher M 2005 *J. Phys.: Condens. Matter* **17** S577
[7] Heslot F, Cazabat A M, Levinson P and Fraysse N 1990 *Phys. Rev. Lett.* **65** 599
[8] Albrecht U, Otto A and Leiderer P 1992 *Phys. Rev. Lett.* **68** 3192
[9] Voué M, Valignat M P, Oshanin G, Cazabat A M and De Coninck J 1998 *Langmuir* **14** 5951
[10] Kavehpour H P, Ovryn B and McKinley G H 2003 *Phys. Rev. Lett.* **91** 196104
[11] Moon J, Lowekamp J, Wynblatt P, Garoff S and Sutter R M 2001 *Surf. Sci.* **488** 73
[12] Moon J, Garoff S, Wynblatt P and Sutter R M 2004 *Langmuir* **20** 402
[13] de Gennes P G and Cazabat A M 1990 *C. R. Acad. Sci.* **310 II** 1601
[14] Oshanin G, De Coninck J, Cazabat A M and Moreau M 1998 *J. Mol. Liq.* **76** 195
[15] Burlatsky S F, Oshanin G, Cazabat A M and Moreau M 1996 *Phys. Rev. Lett.* **76** 86
[16] Abraham D B, Cuerno R and Moro E 2002 *Phys. Rev. Lett.* **88** 206101
[17] De Coninck J 1996 *Colloids Surf.* A **114** 155
[18] Popescu M N and Dietrich S 2004 *Phys. Rev.* E **69** 061602
[19] Popescu M N and Dietrich S 2003 *Interface and Transport Dynamics* ed H Emmerich, B Nestler and M Schreckenberg (Heidelberg: Springer) p 202
[20] Popescu M N and Dietrich S, unpublished
[21] Leung K-t 2000 *Phys. Rev.* E **63** 016102
[22] Giacomin G and Lebowitz J L 1996 *Phys. Rev. Lett.* **76** 1094
[23] Vlachos D G and Katsoulakis M A 2000 *Phys. Rev. Lett.* **85** 3898
[24] Elliott C M and French D A 1987 *IMA J. Appl. Math.* **38** 97
[25] Witelski T P 1995 *Appl. Math. Lett.* **8** 27
[26] Witelski T P 1996 *Stud. Appl. Math.* **96** 277